X-ray-absorption and resonant-photoemission study of Ca in the high-temperature superconductor $Bi_2Sr_2CaCu_2O_8$

M. Qvarford, J. N. Andersen, R. Nyholm, J. F. van Acker, E. Lundgren, and I. Lindau
Department of Synchrotron Radiation Research, Institute of Physics, Lund University, Sölvegatan 14, S-223 62 Lund, Sweden
and MAX-lab, Lund University, Box 118, S-221 00 Lund, Sweden

S. Söderholm, H. Bernhoff, U. O. Karlsson, and S. A. Flodström
Materials Science, Department of Physics, Royal Institute of Technology, S-100 44 Stockholm, Sweden
(Received 4 May 1992; revised manuscript received 10 August 1992)

The electronic structure of Ca in the high-temperature superconductor $Bi_2Sr_2CaCu_2O_8$ has been studied by x-ray-absorption spectroscopy and resonant-photoemission at the Ca $L_{2,3}$ absorption edge. In the x-ray-absorption spectrum no edge structure is seen at the energy corresponding to the Ca $2p_{3/2}$ core-level binding energy, in agreement with the very low Ca density of states at the Fermi level predicted by band-structure calculations. Furthermore, the crystal-field splitting of the Ca $3d$ level, which is characteristic of ionic Ca compounds, is clearly observed in the x-ray-absorption spectrum. The photoemission spectra display strong resonant enhancements of the Ca $3s$ and $3p$ core levels as well as strong changes in the intensity and the line shape of the Ca $L_{2,3}M_{2,3}M_{2,3}$ Auger structure at the Ca $L_{2,3}$ threshold, showing the localized nature of the $3d$ states in core ionized Ca. The $3d$ induced spectator shift of the Ca $L_{2,3}M_{2,3}M_{2,3}$ complex is fairly small as compared to what has been reported for CaF_2, indicating that the screening of the normal Auger final state by the charge carriers in the surrounding Cu-O_2 layers is quite efficient. From the Ca $L_{2,3}M_{2,3}M_{2,3}$ data it is also suggested that, at the Ca L_2 threshold, the excited $3d$ electron participates in a Coster-Kronig-type decay resulting in a $2p_{3/2}$ core hole followed by a normal $L_3M_{2,3}M_{2,3}$ Auger decay.

I. INTRODUCTION

A large number of studies of the high-temperature superconductor (HTS) $Bi_2Sr_2CaCu_2O_8$ during the past years[1] has revealed several characteristic properties of the electronic structure of this multilayered compound. One striking property is a low but clearly detectable density of states (DOS) at the Fermi level (E_F).[2,3] Band-structure calculations[4-7] suggest that the electron bands crossing E_F originate from mainly two of the constituent oxide layers of the superconductor, Cu-O_2 and Bi-O. These calculations show that the bands disperse strongly along the Γ-X and Γ-Y directions, but are almost dispersionless along the Γ-Z direction, displaying a characteristic two-dimensional character of the electronic structure in $Bi_2Sr_2CaCu_2O_8$. A two-dimensional electronic structure is also adopted in the other widely used model of HTS, i.e., the charge-transfer insulator model. In this model the band being responsible for the charge transport arises from hybridized Cu $3d$ and O $2p$ orbitals. The finite density of states at the Fermi level is due to doping-induced hole states which in the charge-transfer model are expected to have mainly O $2p$ character.[8] A confirmation of a two-dimensional character for the O $2p$ holes in $Bi_2Sr_2CaCu_2O_8$ is provided by polarization-dependent absorption measurements[9,10] showing an x,y symmetry of the unoccupied O $2p$ states[11] near the Fermi level. From these facts the HTS $Bi_2Sr_2CaCu_2O_8$ can be qualitatively described as consisting of two-dimensional conducting Cu-O_2 and Bi-O layers separated by rather insulating Ca and Sr-O layers.

The present work is an electron spectroscopy study of Ca in the HTS $Bi_2Sr_2CaCu_2O_8$. According to band-structure calculations,[6] Ca, which is situated between two Cu-O_2 layers, has an "extremely ionic" character. A study of the electronic properties of Ca in this compound is important since it is believed[6] that the strong two-dimensionality in the band description of $Bi_2Sr_2CaCu_2O_8$ is caused by the oxygen-deficient Ca layer. The techniques used are x-ray-absorption spectroscopy (XAS) and resonant photoemission at the Ca $L_{2,3}$ edge. The XAS spectrum provides information about the valence character of Ca in two ways: first, from the comparison between the energy of the absorption onset in the XAS spectrum and the photoemission binding energy, which are expected to coincide in a metallic system, and second, from the crystal-field splitting of the Ca $3d$ states which is expected to be seen in the $L_{2,3}$ edge of more ionic Ca compounds. The XAS results obtained in this study point towards an ionic character of Ca in $Bi_2Sr_2CaCu_2O_8$, in agreement with the band-structure calculations.[6] To gain further insight into the properties of the Ca states[11] above E_F in $Bi_2Sr_2CaCu_2O_8$, resonant-photoemission measurements have been performed at the Ca $L_{2,3}$ absorption edge. From an earlier study of CaF_2,[12] it is known that strong resonance phenomena occur at this edge. This is also found in the present study of Ca in $Bi_2Sr_2CaCu_2O_8$. The Ca $3s$ and $3p$ core levels and the Ca

$L_{2,3}M_{2,3}M_{2,3}$ Auger peak are strongly enhanced at photon energies corresponding to the characteristic peaks in the Ca $L_{2,3}$ absorption spectrum. Some differences between the Ca $L_{2,3}M_{2,3}M_{2,3}$ decay data obtained in the present study and the CaF_2 data of Tiedjie *et al.*[12] are argued to arise from the fact that $Bi_2Sr_2CaCu_2O_8$ is a conductor. Furthermore, strong changes in the line shape of the $L_{2,3}M_{2,3}M_{2,3}$ spectrum at the absorption edge were observed and will be discussed. From the analysis it is suggested that a Coster-Kronig type of decay takes place at the Ca L_2 threshold.

II. EXPERIMENT

The experiments were performed at the soft x-ray beamline 22 at the MAX synchrotron radiation laboratory in Lund, Sweden. This beamline is equipped with a modified SX-700 plane grating monochromator covering the photon energy range of about 20 to 1000 eV. XAS spectra were recorded by detecting the total electron yield. A hemispherical electron energy analyzer (200-mm mean radius) with a multichannel detector system[13] was used to record the photoemission spectra. For the Ca $L_{2,3}$ XAS spectrum the photon energy resolution was 0.2 eV, while the resonant-photoemission spectra were recorded with a photon energy resolution of 0.3 eV and an electron energy resolution of 0.6 eV.[14] An accurate determination of the photon energy scale in the XAS spectra as well as of the photoemission binding energy is vital. For the calibration of the photon energy, we have taken advantage of the radiation in second-order diffraction from the monochromator. At the photon energy at which the absorption edge occurs two photoemission measurements of a corel level were performed, one using first-order light, and another using second-order light. The difference in kinetic energy of the photoemission peak between these two spectra is equal to the photon energy at the absorption edge. The photoemission binding energies were determined with reference to the Fermi edge of a Co sample in electrical contact with the HTS crystal.

$Bi_2Sr_2CaCu_2O_8$ single crystals were glued with conducting silver epoxy to a sample holder. Clean samples were obtained by cleaving *in situ*, which results in a Bi-O surface.[15] The quality of the surface was investigated by low-energy electron diffraction (LEED) which showed the characteristic 5×1 diffraction pattern.[16] A low pressure, about 7×10^{-11} Torr, in the experimental chamber ensured the cleanness of the samples during the experiments. The growth and characterization of the single crystals have been described elsewhere.[17] The superconducting transition temperature of the present samples as determined by magnetic measurements is reported[17] to be 90 K.

III. RESULTS AND DISCUSSION

A. X-ray-absorption spectroscopy

Figures 1(a) and 1(b) show the XAS spectra in the vicinity of the O K and Ca $L_{2,3}$ absorption edges, respectively. These spectra display, due to the dipole selection rules of the x-ray-absorption process, the local empty O p and Ca s,d states. The spectra are measured at a photon incidence angle of 30° with respect to the sample normal, in order to probe electron states both parallel and perpendicular to the crystal surface. The XAS onset corresponds to the creation of a final state where a core electron has been excited from a core level to the lowest unoccupied state. Similarly, in the completely screened core-level photoemission final state in a metal a core electron has been removed and a charge redistribution occurs in which one electron screens the core hole in the lowest unoccupied state. These two final states are thus indistinguishable and the energy onset in the XAS spectrum should, for a metallic system, be equal to the photoemission binding energy. The binding energies for the core levels relevant for the spectra in Fig. 1 are 528.9 eV for the O 1s level and 344.7 eV for the Ca $2p_{3/2}$ level. In Fig. 1 these binding energies are marked by horizontal bars which represent the FWHM (full width half maximum) values obtained by a fit of a single Voigt line profile (O 1s: FWHM=1.9 eV, Ca $2p_{3/2}$: FWHM=1.5 eV) to the core-level peaks. These core-level peaks are most likely composed of several components due to different oxygen sites[18] and a probable Ca-Sr intermixing[19] (cf. discussion

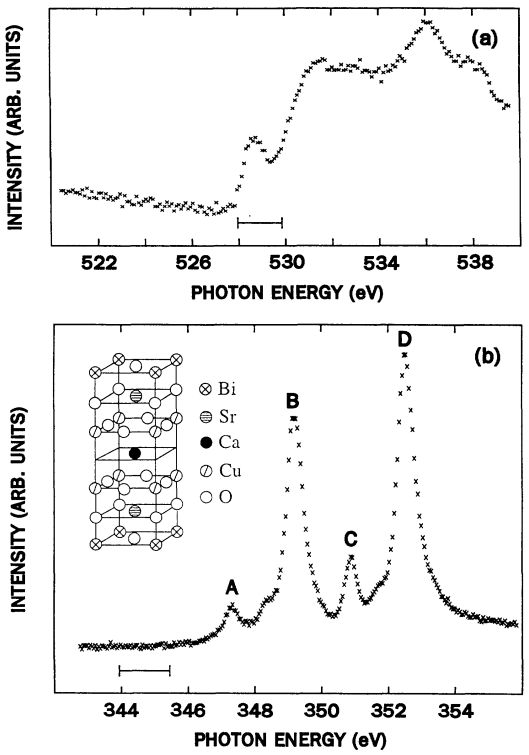

FIG. 1. Total yield XAS spectra at the (a) O K and (b) Ca $L_{2,3}$ thresholds. The photoemission binding energy of the core level excited in the absorption process is marked with a horizontal bar (explanation in text). The peaks denoted A–D in (b) correspond to the photon energies used for spectra A–D in Figs. 4 and 5. The inset in (b) shows the crystal structure of $Bi_2Sr_2CaCu_2O_8$.

below). Thus, the main contribution to the uncertainty in the determination of the binding energies arises from the assignments of the unresolved core-level components. As can be seen in Fig. 1(a) the coincidence of the XAS onset and the photoemission binding energy which is expected for a metallic system is fulfilled at the O K absorption edge. Turning now to the Ca $L_{2,3}$ absorption edge, Fig. 1(b) shows that the XAS onset does not correspond to the photoemission binding energy. From the arguments above this reflects a nonmetallic behavior for Ca in $Bi_2Sr_2CaCu_2O_8$.

It is instructive to discuss the positions of the XAS onsets in the light of the crystal structure and the calculated DOS, even though one should keep in mind that the states probed by XAS are strongly influenced by the presence of the core hole. Several band-structure calculations[4–7] give a Fermi-level DOS primarily originating from the Cu-O_2 and Bi-O planes. The three different oxygen atoms in the structure contribute all together to an O p DOS of 33% (O, s,p,d DOS: 35%) of the total DOS at E_F.[6] The Ca s,d DOS at the Fermi level is calculated to be very low, only about 0.13% (Ca s,p,d DOS: 0.2%) of the total DOS at E_F.[6] Thus, the absence of an onset corresponding to the photoemission binding energy in the Ca $L_{2,3}$ XAS spectrum as well as the onset position characteristic for a metallic system seen in the O K spectrum are both in agreement with what can be expected from the calculated DOS and the doped charge-transfer insulator model. The inset in Fig. 1(b) shows a subunit cell of $Bi_2Sr_2CaCu_2O_8$ as determined by Tarascon *et al.*[20] Ca is located in the center of the submit cell, in an eightfold coordination with respect to oxygen nearest neighbors, and separates the two Cu-O_2 layers. The XAS onsets discussed above are thus consistent with the picture of an ionic Ca layer in between two conducting Cu-O_2 layers, demonstrating the two-dimensionality of the electronic structure in $Bi_2Sr_2CaCu_2O_8$.

The structures in the Ca $L_{2,3}$ XAS spectrum are mainly due to $2p^63d^0$ to $2p^53d^1$ transitions.[21] The fact that four main peaks, A–D, are clearly resolved in the Ca $L_{2,3}$ spectrum in Fig. 1(b) indicates the presence of a crystal field at the Ca site[22,23] and provides additional evidence for the statement that Ca in $Bi_2Sr_2CaCu_2O_8$ behaves in a nonmetallic manner. The splitting between the main peaks (B and D) corresponds roughly to the spin-orbit splitting of the Ca $2p$ core level. The splitting of each threshold in two peaks, A and B for the L_3 threshold and C and D for the L_2 threshold, is related to a crystal-field splitting of the Ca $3d$ levels. This has been shown by, for instance, Himpsel *et al.*[22] for a number of Ca compounds by calculations in a cubic crystal field (O_h symmetry) using an atomic multiplet approach. In their experimental data, Himpsel *et al.*[22] find a clear crystal-field splitting for ionic compounds such as CaO and CaF_2, whereas the Ca $L_{2,3}$ spectra of Ca in metallic environments, such as Ca metal and $CaSi_2$, reveal no sign of a crystal-field splitting. From positions and intensities of peaks A and C it is possible to obtain information about the symmetry and the strength of the crystal field at the Ca site (for a comprehensive discussion of this subject, see Ref. 23). It should be noted that the L_{23} XAS spectrum for Ca in $Bi_2Sr_2CaCu_2O_8$ shows more similarities with CaF_2 (eightfold coordination) than with CaO (sixfold coordination).[22] This agrees well with the fact that Ca in $Bi_2Sr_2CaCu_2O_8$ resides in a nearly cubic eightfold coordination, and suggests that the crystal field at the Ca site in $Bi_2Sr_2CaCu_8O_8$ is roughly comparable to the field in CaF_2. In analogy with the CaF_2 results[22] the peaks splitoff towards lower energy at each threshold, A and C, can then be assigned to e_g orbitals whereas peaks B and D are assigned to t_{2g} orbitals. In the spectrum in Fig. 1(b) a shoulder is visible on the low-energy side of both peaks B and D. Similar spectral features are also found for CaF_2, for which the shoulder at D and part of the shoulder at B could not be explained by the inclusion of the crystal field in O_h symmetry,[22,23] It has been suggested that these components originate from a $2p^63d^04s^1$ to $2p^53d^14s^1$ transition, i.e., from Ca^{1+} ions.[24,25]

In this context it is important to consider the degree of Ca-Sr intermixing and how it will influence the structures in the Ca $L_{2,3}$ XAS spectrum. If such intermixing is present in the sample one would expect the Ca and Sr core-level peaks to be composed of two chemically shifted components since the Ca and Sr sites are inequivalent [cf. inset in Fig. 1(b)]. Kohiki *et al.*[19] have from an x-ray photoemission spectroscopy (XPS) study of a single-crystalline $Bi_2Sr_2CaCu_2O_8$ sample, with a determined stoichiometry of $Bi_2Sr_{1.4}Ca_1Cu_2O_y$, concluded that there is a very high degree of intermixing. The Sr deficiency in their sample can probably enhance the Ca concentration at Sr sites. However, based on the stoichiometry and Sr $3d$ and Ca $2p$ photoemission data[26] of our samples, we believe that the degree of intermixing is lower than proposed in Ref. 19. Assuming that the core-level components are symmetric, we can decompose the Ca $2p_{3/2}$ core level into two components, one at 344.7-eV binding energy and one at 345.7-eV binding energy with an intensity ratio Ca [345.7 eV]/Ca[344.7 eV] of 0.24. In a similar way the Sr $3d_{5/2}$ core level is decomposed into two components at 131.8- and 132.5-eV binding energy with an intensity ratio Sr[132.5 eV]/Sr[131.8 eV] of 0.17. Corresponding intensity ratios reported in Ref. 19 are 0.59 for Ca and 0.25 for Sr. Based on calculations of bond valences Kohiki *et al.*[19] attribute the low binding-energy component (Sr[131.8 eV] and Ca[344.7 eV]) to emission from Sr and Ca atoms occupying Sr sites. This would for the samples in the present study mean that approximately 80% of the Ca atoms would occupy Sr sites, which, given the determined stoichiometry of the present samples, $Bi_{2.10}Sr_{1.94}Ca_{0.88}Cu_{2.07}O_{8+\delta}$,[17] implies that there are 2.37 atoms at Sr sites and 0.45 atoms at Ca site per formula unit, in contradiction to the number of Sr and Ca sites in the subcell structure (Sr: two sites; Ca: one site, see Fig. 1). If it instead is assumed that the Ca component at 344.7-eV binding energy originates from Ca atoms at Ca sites whereas the assignments of the Sr components remain the same as in Ref. 19, this contradiction concerning the number of Ca and Sr sites in the stoichiometric cell is avoided. Hence, it is suggested that approximately 20% of the Ca atoms in the present sam-

ples may occupy Sr sites. This should be regarded as an upper limit since any asymmetry in the core-level components will further decrease this estimate of the intermixing.

As mentioned above it has been suggested[24,25] that the weak structure at the low energy side of the main peaks B and D in the Ca $L_{2,3}$ spectrum originates from Ca ions with valence Ca^{+} instead of Ca^{2+}. A downward energy shift of the absorption edge induced by such a valence change has been confirmed by atomic multiplet calculations[22] and has been observed at the CaF_2/Si(111) interface[22] as well as at defects (F centers) at the CaF_2 surface.[22] A second cause for structures on the low-energy side of the main absorption peaks found for CaF_2 (Ref. 22) is the lower symmetry at the surface. It can, for Ca in $Bi_2Sr_2CaCu_2O_8$, be speculated that the most probable cause for these extra structures in the Ca $L_{2,3}$ spectrum is the lower symmetry experienced by Ca atoms at Sr sites (cf. Fig. 1). The facts that these structures are so weak and that the overall Ca $L_{2,3}$ edge looks so much like what is expected for a cubic surrounding support the proposed low intermixing of Ca atoms in Sr sites. We will not discuss these weak structures in the Ca $L_{2,3}$ XAS spectrum further here. The important conclusion we want to stress is that one for Ca in $Bi_2Sr_2CaCu_2O_8$ sees a crystal-field splitting in the Ca $L_{2,3}$ XAS spectrum, a splitting which is characteristic for ionic Ca compounds but not for metallic Ca.

B. Resonant photoemission

In resonant photoemission, changes of the electron emission in the vicinity of a photoabsorption threshold of a deeper lying core level are investigated. The spectral features of concern in the present work, using excitation energies around the Ca $L_{2,3}$ absorption edge, have been the Ca $L_{2,3}M_{2,3}M_{2,3}$ Auger and the Ca $3s$ and Ca $3p$ photoemission peaks. Figure 2 displays the overall behavior of these Ca related features when the photon energy is scanned through the Ca $L_{2,3}$ edge. The plot is dominated by a very high intensity of the $L_{2,3}M_{2,3}M_{2,3}$ emission ($50 < E_b < 70$ eV) at photon energies corresponding to the main Ca $L_{2,3}$ peaks, but also resonances in the $3p$ ($E_b = 23$ eV) and $3s$ ($E_b = 42$ eV) photoemission are clearly seen. The inset pictures two different decay processes involving the $3p$ level following the $L_{2,3}$ absorption process. In the spectator decay the excited electron stays in a localized $3d$ orbital during the subsequent $L_{2,3}M_{2,3}M_{2,3}$ decay.[27] In the participator decay the excited electron takes part in the $2p$ core hole decay, giving a final state which is degenerate with the Ca $3p$ photoemission at the resonant photon energy. The three-dimensional plot in Fig. 2 shows the birth of the Ca $L_{2,3}M_{2,3}M_{2,3}$ Auger. At the low photon energy side, below the L_3 threshold, the spectrum is completely flat in the energy range of this Auger decay. As the photon energy increases very strong intensity enhancements are seen at energies corresponding to the Ca $L_{2,3}$ peaks A–D [cf. Fig. 1(b)], followed at higher photon energies by the development of the normal Ca $L_{2,3}M_{2,3}M_{2,3}$ Auger. In addition to the enhanced features discussed so far, another enhanced feature between the Ca $3s$ and Ca $3p$ peaks is seen in Fig. 2. Since a Ca Auger in the energy region between the $3s$ and $3p$ participator decays is not possible without involving a valence electron, it is attributed to the Ca $L_{2,3}M_{2,3}V$ Auger decay.[28]

The participator processes are seen as enhancements of the Ca $3p$ and $3s$ photoemission peaks. These enhancements are shown in more detail in the CIS (constant initial state) spectra in Fig. 3. The CIS spectra represent cuts parallel to the photon energy axis at the Ca $3p$ and

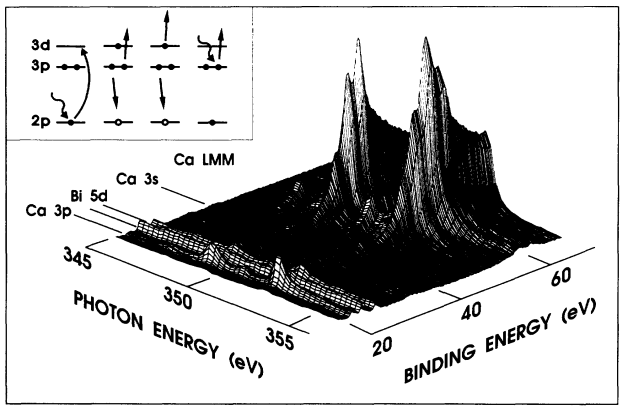

FIG. 2. Three-dimensional plot of the photoemission intensity in the binding-energy range 20–70 eV as a function of photon energy close to Ca $L_{2,3}$ absorption edge. The plot is dominated by the high intensity in the $L_{2,3}M_{2,3}M_{2,3}$ emission. The inset shows the different processes studied in the vicinity of the Ca $L_{2,3}$ absorption edge. From left to right: the x-ray-absorption process, the $L_{2,3}M_{2,3}M_{2,3}$ spectator process, the $3p$ participator process, and the normal $3p$ photoemission with which the participator process is degenerate at the x-ray-absorption threshold.

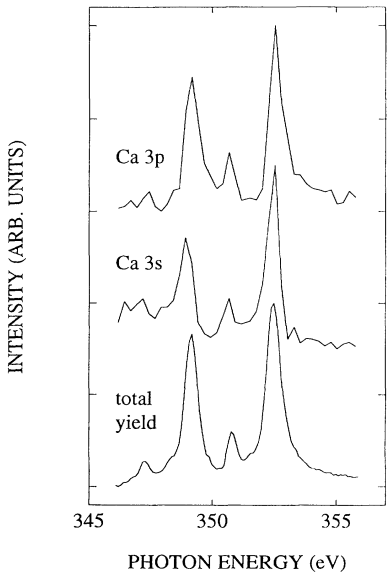

FIG. 3. CIS spectra at the Ca $L_{2,3}$ edge for the Ca $3p$ and $3s$ core levels. At the bottom is also shown the Ca $L_{2,3}$ total yield spectrum.

3*s* binding-energy positions in Fig. 2 and give a measure of the photon energy-dependent cross section for the Ca 3*p* and 3*s* photoemission. The total yield XAS spectrum at the Ca $L_{2,3}$ edge is shown, for comparison, at the bottom of Fig. 3. These spectra reveal that the enhancements of the Ca 3*p* and 3*s* photoemission are strongly related to the XAS intensity, and demonstrate the high degree of localization of the excited 3*d* electrons.

Figure 4 shows photoemission spectra, covering the Ca $L_{2,3}M_{2,3}M_{2,3}$ Auger region and the Ca 3*s* and 3*p* photoemission peaks, measured with photon energies corresponding to peaks $A-D$ in the Ca $L_{2,3}$ spectrum in Fig. 1(b), i.e., the photon energies at which the cross section for creating a 2*p* core hole is largest. These spectra represent cuts parallel to the binding energy axis in Fig. 2 (plotted on a kinetic-energy scale for convenience while discussing the spectator decay), and are normalized to the photon flux. For comparison a spectrum measured off resonance, above the Ca $L_{2,3}$ edge (356-eV photon energy), is shown at the top of Fig. 4. The Bi 5*d* levels at a kinetic energy just below the Ca 3*p* peak may be used as a guide to the eye when comparing the relative intensities of the resonating features.[29] From the spectra it is obvious that there is a strong general enhancement of the Ca related features at the main absorption peaks.

The occurrence of the Ca 3*p* participator decay settles the question about the binding energy, $E_b=23.2$ eV, for this core level in $Bi_2Sr_2CaCu_2O_8$, which has been subject of discussion in earlier work[30] due to the large number of different core levels in this spectral region. The resonant-photoemission data also provide a value for the Ca 3*s* binding energy, $E_b=41.7$ eV. The peak at around 5 eV above the Ca 3*s* peak is the Sr 4*s* core level. The enhanced feature at a kinetic energy slightly below 320 eV seen in spectra *B* and *D* is attributed to the Ca $L_{2,3}M_{2,3}V$ Auger as discussed above. The most pronounced enhancement is seen for the Ca $L_{2,3}M_{2,3}M_{2,3}$ Auger at a kinetic energy of around 295 eV.

In Fig. 5, the Ca $L_{2,3}M_{2,3}M_{2,3}$ to Ca 3*s* region of the spectra in Fig. 4 is shown, normalized to equal peak intensity. First it can be noted from these spectra that large changes in the spectral line shape of the $L_{2,3}M_{2,3}M_{2,3}$ decay channel occur at the $L_{2,3}$ threshold. Furthermore, by inspecting the energy positions of the $L_{2,3}M_{2,3}M_{2,3}$ peaks in spectra *C* and *D* (when both spin-orbit components of the 2*p* core level are excited) it is seen that these peaks are slightly shifted towards higher kinetic energy as compared to the $L_{2,3}M_{2,3}M_{2,3}$ Auger peak measured above the absorption edge (top spectrum). This shift can, from the spectra in Fig. 5, be estimated to 2–3 eV (cf. discussion below). A spectator shift towards higher kinetic energy is expected since a localized 3*d* electron will screen the final-state 3*p* holes. By comparing the spectra in Fig. 5 to similar spectra measured for CaF_2,[12] it is found that the spectator shift for Ca in $Bi_2Sr_2CaCu_2O_8$ is about 4–5 eV smaller than for Ca in CaF_2. The smaller spectator shift found in $Bi_2Sr_2CaCu_2O_8$ as compared to CaF_2 indicates that, even though the Ca layer in $Bi_2Sr_2CaCu_2O_8$ has a local ionic character as concluded from the Ca $L_{2,3}$ XAS spectrum, the screening of the normal Auger final state by the

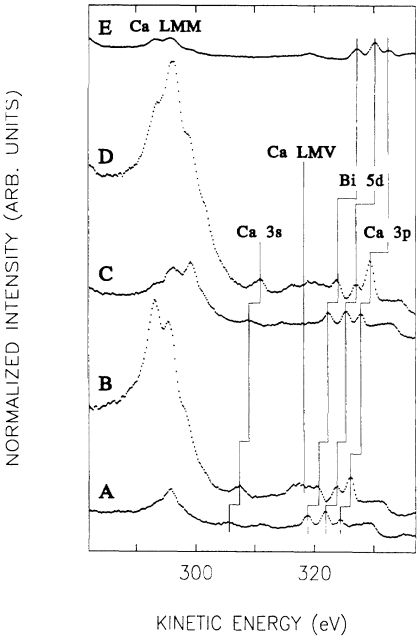

FIG. 4. Photoemission spectra at the Ca $L_{2,3}$ absorption edge (see text for details). Spectra $A-D$ are measured at photon energies corresponding to the peaks $A-D$ in the Ca $L_{2,3}$ XAS spectrum in Fig. 1(b), whereas spectrum *E* is measured at a photon energy (356 eV) above the Ca $L_{2,3}$ threshold. The spectra are normalized to the photon flux.

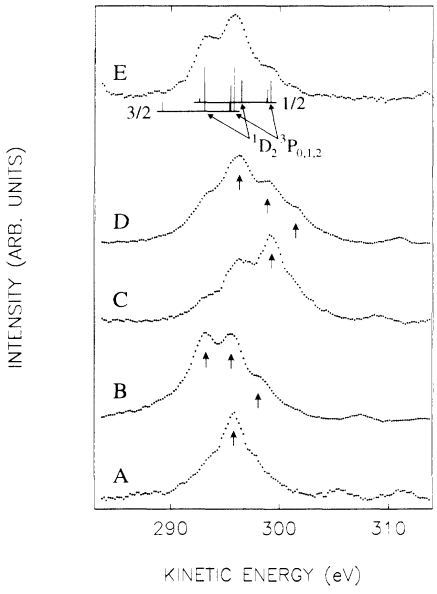

FIG. 5. The Ca $L_{2,3}M_{2,3}M_{2,3}$ Auger region of the spectra in Fig. 4. The spectra are normalized to equal peak intensity, and a Shirley background has been subtracted. The small peak on the high-energy side of the spectra is the Ca 3*s* core level. In the bottom spectra the Sr 4*s* core level at about 311 eV can also be seen. A calculated atomic Auger multiplet is shown as vertical bars in spectrum *E*.

charge carriers in the surrounding $Cu\text{-}O_2$ layers must be quite efficient.

In order to further analyze the line shape of the Ca $L_{2,3}M_{2,3}M_{2,3}$ decay channel, the atomic Auger multiplet structure for a $3p^4$ final state has been calculated. The calculation is performed using an atomic multiconfigurational Dirac-Fock program.[31] The intermediate coupling scheme gives for this final state a multiplet split into $^1S_0$, $^1D_2$ and $^3P_{0,1,2}$ term levels (in order of increasing energy). The calculated atomic Auger multiplet is shown, using relative intensities proportional to the multiplicities, as vertical bars in the normal Auger spectrum in Fig. 5 for both the $2p_{3/2}$ and $2p_{1/2}$ initial states, the $\frac{3}{2}$ component at lower energy and the $\frac{1}{2}$ component at higher energy. The $2p$ spin-orbit splitting is experimentally determined to be 3.5 eV. As seen there is good agreement between the calculated and the measured peak structure.

In the pure spectator model it is assumed that the only effect of the $3d$ spectator electron is to shift the overall spectrum,[32] i.e., the spectator electron does not cause any additional multiplet effects. Applying this model to spectra $A-D$ in Fig. 5, taking only the $\frac{3}{2}$ component of the calculated Auger spectrum into account for spectra A and B and both the $\frac{3}{2}$ and $\frac{1}{2}$ components for spectra C and D, one may fit the main lines $^1D_2$ and $^3P_{0,1,2}$ fairly well in energy position to structures in spectra $A-D$. This procedure would give a spectator shift of approximately 2–3 eV, in agreement with the value given above. In addition to this shift there are strong variations in the Ca $L_{2,3}M_{2,3}M_{2,3}$ line shape at the Ca $L_{2,3}$ threshold, as can clearly be seen by a comparison of spectra $A-D$ in Fig. 5. These intensity changes cannot be explained within the pure spectator model, since one must allow for strong variations in the intensity of the multiplet lines to get accurate fits to the data. Another possibility, which has been proposed for CaF_2,[12] is that the intensity changes at the low-energy side of the spectra are due to shakeup or shakeoff processes in which the spectating $3d$ electron becomes further excited or ionized during the $L_{2,3}M_{2,3}M_{2,3}$ decay. The applicability of this explanation to some of the structures in spectra C and D will be discussed below. If the main assumption in the pure spectator model is not valid, the Auger final state will be a $3p^43d^1$ state with a multiplet structure containing 28 lines. Such a breakdown of the spectator model in its most simple form has been found for atomic Ar, K, and Ca.[33]

Finally, it can be seen in Fig. 5 that the main structures in spectra A and B, marked with arrows, are also found, although shifted by the spin-orbit splitting, in spectra C and D, respectively. This behavior, and the difference between spectra A and B suggest that the spectator decays are equal at the L_3 and L_2 thresholds, but that they differ with respect to the situation where the spectator electron is in the e_g state (spectra A and C) or in the t_{2g} state (spectra B and D). However, it is also clearly seen that spectra C and D are not simply shifted replicas of spectra A and B; in C and D additional intensity is found at the low kinetic-energy side of the marked structures. The cross section for directly creating a $2p_{3/2}$ core hole by x-ray absorption at the L_2 threshold is very small [cf. Fig. 1(b)], so it is unlikely that all this additional intensity arises from a direct $L_3M_{2,3}M_{2,3}$ decay. Furthermore, any explanation including production of L_3 holes by direct photoabsorption seems incapable of explaining the fact that these extra structures are more intense in spectrum D as compared with spectrum C (see Fig. 4). Another suggestion could be that they arise from shakeup processes during the $L_2M_{2,3}M_{2,3}$ decay. But such processes might just as well occur at the L_3 threshold and should then be seen as similar low-energy structures in spectra A and B. Neither of these explanations of the additional low-energy structures in spectra C and D are thus probable. In order to further analyze this features we display in Fig. 6 a series of spectra constructed in the following way: Spectrum 1 is the result of a subtraction of spectrum A in Fig. 5, shifted by the spin-orbit split to higher kinetic energy, from spectrum C in Fig. 5. Spectrum 2 in Fig. 6 is obtained in a similar way, but now with the use of spectra B and D in Fig. 5. Spectrum 3 in Fig. 6 is obtained by application of a decomposition algorithm[34] to the normal Auger spectrum, yielding the $2p_{3/2}$ related part of spectrum E in Fig. 5. As is seen in Fig. 6 these three constructed spectra are similar with two main structures at about 295 and 293 eV, indicating that the additional low-energy structures in spectra C and D are actually due to an enhancement of the $L_3M_{2,3}M_{2,3}$ normal Auger component at the L_2 thresholds. This demands a strongly enhanced probability of creating $2p_{3/2}$ core holes at the L_2 threshold, and implies, because of the above considerations concerning the direct production of L_3 holes, that a Coster-Kronig type of decay takes place at this threshold. In this process the $2p_{1/2}$ core

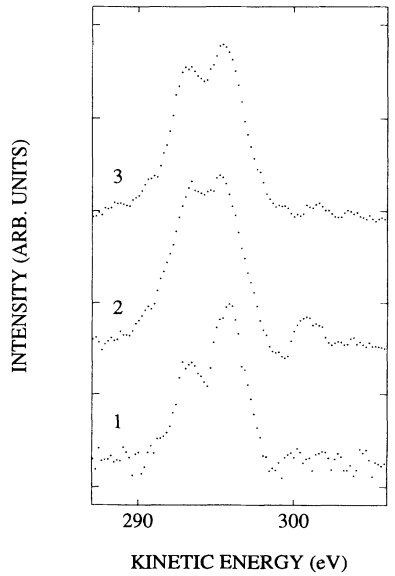

FIG. 6. Spectra 1–3 display the $2p_{3/2}$ related part of spectra $C-E$ in Fig. 5. The spectra are constructed using subtraction procedures as described in the text, and are normalized to equal peak intensity.

hole is filled by a $2p_{3/2}$ electron giving the energy corresponding to the spin-orbit splitting, approximately 3.5 eV, to the $3d$ spectator electron. The subsequent decay is then a normal Ca $L_3M_{2,3}M_{2,3}$ Auger decay. In CaF_2 the estimated binding energy relative to the conduction band edge of the $3d$ electron in the XAS final state is about 3.7 eV,[12] a fact which makes this type of Coster-Kronig decay less probable for CaF_2.

IV. SUMMARY

In summary we have by XAS probed the local unoccupied Ca states in $Bi_2Sr_2CaCu_2O_8$. The absence of a clear absorption edge at the energy corresponding to the Ca $2p_{3/2}$ binding energy in the Ca $L_{2,3}$ spectrum is in agreement with what is expected from band-structure calculations, and is in contrast to the correspondence of the XAS onset with the core-level binding energy seen for the O K XAS spectrum. The crystal-field splitting of the $3d$ states in the Ca $L_{2,3}$ spectrum lends further support to the notion of an ionic Ca layer in $Bi_2Sr_2CaCu_2O_8$. Resonant photoemission at the Ca $L_{2,3}$ edge gives additional information about the local unoccupied d states for core ionized Ca. The occurrence of participator and spectator Auger decays of the Ca $2p$ core hole shows that the Ca $3d$ states are localized in the presence of a $2p$ core hole. Furthermore, the small spectator shift as compared to CaF_2 indicates that the screening at the Ca site provided by the conducting Cu-O_2 layers is quite efficient. Moreover, from the identification of an $L_3M_{2,3}M_{2,3}$ component in spectra measured at the L_2 threshold, it is suggested that a Coster-Kronig type of decay involving the excited $3d$ electron takes place at this threshold.

ACKNOWLEDGMENTS

We thank Dr. Z-X. Shen for providing the single crystals and for useful discussions. This work was supported by the Swedish Natural Science Research Council and the Swedish National Board for Technical Development.

[1]For a review, see, for example, P. A. P. Lindberg, Z.-X. Shen, W. E. Spicer, and I. Lindau, Surf. Sci. Rep. **11**, 1 (1990).

[2]H. M. Meyer, III, D. M. Hill, J. H. Weaver, D. L. Nelson, and C. F. Gallo, Phys. Rev. B **38**, 7144 (1988).

[3]H. Bernhoff, M. Qvarfold, S. Söderholm, A. S. Flodström, J. N. Andersen, R. Nyholm, U. O. Karlsson, and I. Lindau, Physica C **180**, 120 (1991).

[4]H. Krakauer and W. E. Pickett, Phys. Rev. Lett. **60**, 1665 (1988).

[5]M. S. Hybertsen and L. F. Mattheiss, Phys. Rev. Lett. **60**, 1661 (1988).

[6]S. Massida, Jaejun Yu, and A. J. Freeman, Physica C **152**, 251 (1988).

[7]P. A. Sterne and C. S. Wang, J. Phys. C **21**, L949 (1988).

[8]See, for example, G. A. Sawatsky, in *Earlier and Recent Aspects of Superconductivity,* edited by J. G. Bednorz and K. A. Müller, Springer Series in Solid State Sciences Vol. 90 (Springer-Verlag, Berlin, 1990), p. 345, and references therein.

[9]F. J. Himpsel, G. V. Chandrashekhar, A. B. McLean, and M. W. Shafer, Phys. Rev. B **38**, 11 946 (1988).

[10]N. Nücker, H. Romberg, X. X. Xi, J. Fink, B. Gegenheimer, and Z. X. Zhao, Phys. Rev. B **39**, 6619 (1989).

[11]With "states" we mean the electron states probed in the presence of the core hole created in the x-ray-absorption process.

[12]T. Tiedje, K. M. Colbow, D. Rogers, and W. Eberhardt, Phys. Rev. Lett. **65**, 1243 (1990).

[13]J. N. Andersen, O. Björneholm, A. Sandell, R. Nyholm, J. Forsell, L. Thånell, A. Nilsson, and N. Mårtensson, Synch. Rad. News **4**, No. 4, 15 (1991).

[14]Measurements with an electron energy resolution of 0.3 eV did not result in considerably sharper spectral structures.

[15]See, for example, P. A. P. Lindberg, Z.-X. Shen, B. O. Wells, D. S. Dessau, D. B. Mitzi, I. Lindau, W. E. Spicer, and A. Kapitulnik, Phys. Rev. B **39**, 2890 (1989).

[16]P. A. P. Lindberg, Z.-X. Shen, B. O. Wells, D. B. Mitzi, I. Lindau, W. E. Spicer, and A. Kapitulnik, Appl. Phys. Lett. **53**, 2563 (1988).

[17]D. B. Mitzi, L. W. Lombardo, A. Kapitulnik, S. S. Laderman, and R. D. Jacowitz, Phys. Rev. B **41**, 6564 (1990).

[18]F. Parmigiani, Z. X. Shen, D. B. Mitzi, I. Lindau, W. E. Spicer, and A. Kapitulnik, Phys. Rev. B **43**, 3085 (1991).

[19]S. Kohiki, T. Wada, S. Kawashima, H. Takagi, S. Uchida, and S. Tanaka, Phys. Rev. B **38**, 7051 (1988).

[20]J. M. Tarascon, W. R. McKinnon, P. Barboux, D. M. Hwang, B. G. Bagley, L. H. Greene, G. W. Hull, Y. LePage, N. Stoffel, and M. Giroud, Phys. Rev. B **38**, 8885 (1988).

[21]M. W. D. Mansfield, Proc. R. Soc. London, Ser. A **348**, 143 (1976).

[22]F. J. Himpsel, U. O. Karlsson, A. B. McLean, L. J. Terminello, F. M. F. de Groot, M. Abbate, J. C. Fuggle, J. A. Yarmoff, B. T. Thole, and G. A. Sawatzky, Phys. Rev. B **43**, 6899 (1991).

[23]F. M. F. de Groot, J. C. Fuggle, B. T. Thole, and G. A. Sawatzky, Phys. Rev. B **41**, 928 (1990).

[24]D. Rieger, F. J. Himpsel, U. O. Karlsson, F. R. McFreely, J. F. Morar, and J. A. Yarmoff, Phys. Rev. B **34**, 7295 (1986).

[25]F. J. Himpsel, U. O. Karlsson, J. F. Morar, D. Rieger, and J. A. Yarmoff, Phys. Rev. Lett. **56**, 1497 (1986).

[26]The Sr $3d$ core levels were measured at 250-eV photon energy and a total energy resolution of 0.3 eV whereas the Ca $2p$ core levels were measured at 500-eV photon energy and a total energy resolution of 0.6 eV.

[27]If the excited electron is not localized, i.e., the core hole decay is not influenced by a spectator electron, the result is a normal Auger decay, i.e., not shifted and with a similar shape to the one observed for excitation energies above the $L_{2,3}$ threshold.

[28]This resonantly enhanced $L_{2,3}M_{2,3}V$ emission has, for CaF_2, been attributed to an interatomic Auger decay involving a F $2p$ electron, see T. Tiedje, K. M. Colbow, D. Rogers, and W. Eberhardt, Phys. Scr. **41**, 621 (1990).

[29]From Fig. 2 it may appear that the Bi $5d$ levels are also

resonating at the characteristic energies of the Ca $L_{2,3}$ edge. This is explained by the fact that the Bi $5_{5/2}$ level rides on the inelastic tail of the Ca $3p$ resonance and the Bi $5d_{3/2}$ level partly coincides with the Ca $L_{2,3}M_{2,3}V$ peak, and is thus not a real photoemission resonance.

[30]R. Manzke, T. Buslaps, R. Claessen, G. Mante, and Z. X. Zhao, Solid State Commun. **70**, 67 (1989).

[31]I. P. Grant, B. J. McKenzie, P. H. Norrington, D. F. Mayers, and N. C. Pyper, Comput. Phys. Commun. **21**, 207 (1980).

[32]An example of a pure spectator shift (in CO) is given in W. Eberhardt, E. W. Plummer, C. T. Shen, and W. K. Ford, Aust. J. Phys. **39**, 853 (1986).

[33]M. Meyer, E. von Raven, M. Richter, B. Sonntag, and J. E. Hansen, J. Electron Spectrosc. Relat. Phenom. **51**, 407 (1990).

[34]R. Nyholm and N. Mårtensson, Chem. Phys. Lett. **74**, 337 (1980).

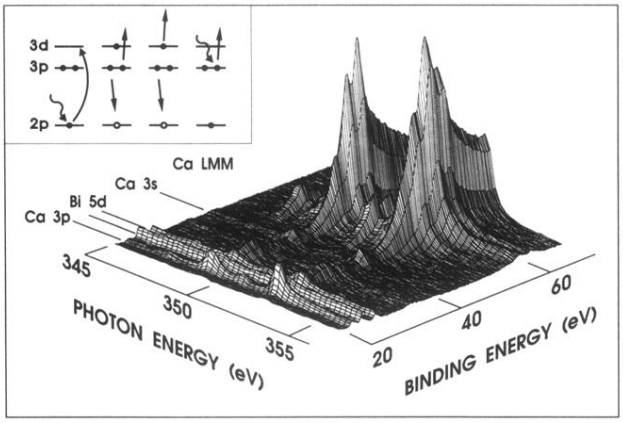

FIG. 2. Three-dimensional plot of the photoemission intensity in the binding-energy range 20–70 eV as a function of photon energy close to Ca $L_{2,3}$ absorption edge. The plot is dominated by the high intensity in the $L_{2,3}M_{2,3}M_{2,3}$ emission. The inset shows the different processes studied in the vicinity of the Ca $L_{2,3}$ absorption edge. From left to right: the x-ray-absorption process, the $L_{2,3}M_{2,3}M_{2,3}$ spectator process, the $3p$ participator process, and the normal $3p$ photoemission with which the participator process is degenerate at the x-ray-absorption threshold.